NUMERICAL STUDY OF TURBULENT MANOEUVRING-BODY WAKES: INTERACTION WITH A FREE SURFACE

Watchapon Rojanaratanangkule, T. Glyn Thomas and Gary N. Coleman
School of Engineering Sciences
University of Southampton
Highfield, Southampton, Hampshire, SO17 1BJ, UK
wr1e09@soton.ac.uk, t.g.thomas@soton.ac.uk and g.n.coleman@soton.ac.uk

ABSTRACT

Direct Numerical Simulation (DNS) is used to investigate the interaction of a turbulent wake, created by an impulsively accelerating axisymmetric self-propelled body, below a free surface. The manoeuvring body is represented by the combination of an immersed boundary method and a body force. The Reynolds number based on either the diameter of the body or the jet forcing intensity is relatively high $(O(1000))$, corresponding to the fully turbulent case. The vertical growth of the coherent structure behind the body is restricted by the upper and lower stress-free layers and the wake signatures are observed to penetrate to the free surface.

INTRODUCTION

Turbulent wakes behind a bluff body have been investigated both experimentally and numerically by many researchers in order to obtain better understanding of their dynamics. However, almost all of the studies have focused on wakes behind towed or self-propelled objects moving at constant velocity. When a body is towed, it imparts momentum, equal to the drag of the body, to the wake. In contrast, for a constant speed self-propelled body, the drag is cancelled by the thrust, leading to a zero-momentum wake.

In practice, a submerged vehicle leaves behind it a finite-momentum wake when it accelerates or changes direction, and a momentumless wake only when it moves at constant speed (Tennekes & Lumley, 1972). A manoeuvring-body wake is of interest because it can introduce dynamics that are absent from the constant-velocity case, especially when the wake is influenced by stable stratification or by the presence of an adjacent free surface. For example, dipole vortices produced by the interaction of manoeuvring-body wakes with either stable background density stratification or a free surface can be observed in geophysical flows (e.g. Ahlnäs *et al.*, 1987; Sous *et al.*, 2004; Voropayev *et al.*, 2007). The practical importance of the dipole vortices is that they are very large, compared to the size of the body, and long-lived. Voropayev *et al.* (1999) estimate that a coherent kilometre-scale vortical structure that persists for the order of days can be observed behind a typical submarine manoeuvre in the ocean. Moreover, due to the self-propelling motion of the dipole vortex, it can transport mass, momentum and other scalar properties such as heat and salt.

Generally, when momentum is imparted into a flow, it leads to an isolated region which possesses a high concentration of vorticity and a non-zero net linear momentum, often referred to as a turbulent blob. In an unbounded homogeneous fluid, the turbulent blob is fully three-dimensional. While the blob is propagating away from its origin, its vertical and horizontal sizes increase due to the entrainment process of the surrounding fluid and the blob eventually transforms into a toroidal vortical structure (Maxworthy, 1977). In contrast, when the vertical growth of the blob is confined (e.g. by buoyancy force or flow geometry), only its horizontal size can expand due to the lateral entrainment, which leads to a quasi-planar counter-rotating vortex.

The formation and evolution of vortex dipoles were widely studied in a linearly stratified fluid (Voropayev *et al.*, 1991; Flór & Van Heijst, 1994; Flór *et al.*, 1995) and have recently been extended to the case of shallow water above a solid surface, for which the vertical size of a turbulent blob is suppressed by the flow geometry. It was found from the experimental study of Sous *et al.* (2004) that the condition in which the momentum disturbance can coherently penetrate upward and produce its signature at the free surface depends on the *confinement number* $C = J^{1/2}\Delta t_f/h^2$, where J is the forcing intensity, h is the depth of the fluid domain, and Δt_f is the forcing interval. The formation and evolution of the vortex dipoles formed in shallow water are similar to those in a stratified fluid except that three-dimensional small scale turbulence appears at the dipole front. Sous *et al.* (2004) stated that the vertical motion at the frontal region might appear due to the effect of bottom friction.

Voropayev *et al.* (2007) performed experiments in a two-layer fluid, where unstratified water was placed above a layer of salt water, in order to reduce the effect of the bottom surface. Their flow geometry is similar to the real upper ocean in which denser water rests underneath a nominally constant density gradient (depth $50-100$ m). They investigated the intensity of the surface signature in terms of the *contrast number* $Cn = \omega_z^*/\langle\omega_z\rangle$, defined as the ratio of the maximum vertical vorticity ω_z^* of the dipole vortex to the root-mean-square value of the background vertical vorticity $\langle\omega_z\rangle$, and also defined a relationship between the confinement number and the

intensity of the surface signature.

The aim of this work is to investigate the evolution of the impulsively submerged momentum disturbance in the small-scale upper ocean, which is mimicked by stress-free top and bottom layers. Two different types of momentum sources are chosen: (1) an impulsive jet and (2) an accelerating motion of a self-propelled body.

NUMERICAL APPROACH

The details of the code used to simulate the evolution of a turbulent blob created by either an impulsive jet or an impulsively accelerating axisymmetric self-propelled body are described below.

We make use of the continuity and the incompressible Navier-Stokes equations in a Cartesian coordinate system x_i, written in Cartesian tensor notation as

$$\frac{\partial u_i}{\partial x_i} = 0, \tag{1}$$

$$\frac{\partial u_i}{\partial t} + u_j \frac{\partial u_i}{\partial x_j} = -\frac{1}{\rho}\frac{\partial p}{\partial x_i} + \nu \frac{\partial^2 u_i}{\partial x_j \partial x_j} + f_i\,, \tag{2}$$

where u_i represents the velocities, t denotes the time, p is the pressure, ρ and ν are respectively the fluid density and kinematic viscosity (which are taken to be constant during the calculations), and f_i is the external body forces which is split into boundary forces due to the virtual body surface $\mathbf{B} = (B_x, B_y, B_z)$ and thrust $\mathbf{T} = (T_x, 0, 0)$.

The Navier-Stokes equations are advanced in time with the second-order explicit Adams-Bashforth scheme. A second-order central finite-difference scheme is used to discretize the spatial derivatives on a staggered grid, where the velocity components are defined at the cell faces while the scalar quantity (pressure) is located in the cell centre (Archer *et al.*, 2008). The continuity equation is imposed via a standard pressure-correction method. The resulting Poison equation for the pressure is solved using a multigrid method.

In order to embed an axisymmetric body into a computational grid, an immersed boundary technique is employed. The boundary forces B_i, which enforce the no-slip boundary condition on the embedded body surface, are calculated directly at the Lagrangian (virtual surface) points via a proportional controller with the proportional gain related to the time step size Δt, in such a way that maximises gain while maintaining stability. The boundary forces are then transformed into the Eulerian (computational) points by using the three-point discrete delta function proposed by Roma *et al.* (1999).

We emulate the body manoeuvre by imposing a thrust, which is modelled as a jet from the body, at its rear. The intensity of the thrust is estimated as

$$J_T = u_{jet} s \left(u_{jet} - U(t)\right)\,, \tag{3}$$

where u_{jet} is the jet velocity, s is the area of the nozzle, and $U(t)$ is the velocity of the body. A three-dimensional Gaussian function is used to distribute the intensity of the thrust to the computational grids as

$$T_x = \frac{J_T}{\left(\delta^2\pi\right)^{3/2}} \exp\left[-\frac{r^2}{\delta^2}\right]\,, \tag{4}$$

where $r^2 = (x-x_o)^2 + (y-y_o)^2 + (z-z_o)^2$, δ is the Gaussian semi-width, and x_o, y_o, z_o are the centre of the thrust. The velocity of the body can be found via the balance of momentum between a manoeuvring object of mass M and the total force acting on the fluid, with

$$(1+k)M\frac{\mathrm{d}U}{\mathrm{d}t} = \rho\left(J_T - J_D\right)\,, \tag{5}$$

where $M = \rho V$, V is the volume of the body, k is the virtual mass coefficient, and J_D is the intensity of the drag, which can be calculated from the volume integral of the streamwise boundary force B_x. An explicit Euler method is used to update $U(t)$ at every time step.

In order to simulate the motion of a manoeuvring body, inflow and outflow boundary conditions are employed in the streamwise (x) direction. Additionally, we perform the calculation in an unsteady moving reference frame in order to maintain the location of the body within the computational box. The uniform inflow velocity is thus set equal to the velocity of the body and is updated every time step. The body is placed midway between a thermocline and a free surface. Hence stress-free boundary conditions are specified at the bottom as an idealisation of the top of a region of a stratified fluid. Periodic conditions are specified in the lateral (y) direction.

When the code is used to study the evolution of an impulsive jet, the boundary forces are turned off and the inflow velocity is set to zero.

RESULTS

In this section we present results from wakes created by an external body force. First, a two-dimensional (2D) momentumless wake is considered to validate the concept of a force doublet. Second, the evolution of the momentum disturbance, created by an impulsive jet, in an unbounded domain and near a free surface is studied. Finally, early results from a turbulent wake behind an impulsively accelerating self-propelled body are presented.

2D Zero-momentum wakes

We validated the concept of a force doublet (drag of the body plus thrust) by performing a 2D simulation of zero-momentum wakes. The results are compared with both an analytical solution (Afanasyev, 2004) and experimental results of Afanasyev & Korabel (2006), who used an electromagnetic force to create zero-momentum wakes in a stratified fluid. For the validation, we used a Gaussian function to distribute the thrust and drag forces. The drag is applied slightly in front of the thrust. Moreover, the thrust and drag forces are defined to be of equal magnitude to generate a momentumless wake. The 2D domain size was 240×80 (in units of 2δ) with 3072×1024 grid points in streamwise and vertical directions

respectively. Figure 1a displays the distribution of the streamwise velocity along the axis of the flow for $\Pi_a = \tilde{J}/aU_\infty^2 = 1$ and $\Pi_\nu = \tilde{J}/\nu U_\infty = 50$, where $\tilde{J}$ is the 2D forcing intensity (force per unit area), a is the forcing area and is equal to the Gaussian semi-width, and U_∞ is the free-stream velocity, compared with an analytical solution (Afanasyev, 2004). Away from the expected near-field deviation (due to comparing finite versus singular dipoles) the agreement is satisfactory. For a quantitative comparison with the laboratory experiment (Afanasyev & Korabel, 2006), the shedding frequency f_s was measured by performing a Fourier transform of the mean value of vorticity at $x/2\delta = 12.5$. The nondimensional frequency, Strouhal number $St = f_s\tilde{J}/U_\infty^3$, versus Π_a is displayed in figure 1b, showing that the numerical results are in good agreement with the experimental data (Afanasyev & Korabel, 2006). The vorticity distribution for $\Pi_a = 11$ and $\Pi_\nu = 230$ is illustrated in figure 2. The vortex street in this simulation is visually similar to the mushroom-like vortex sheet observed in Afanasyev & Korabel's (2006) experiment.

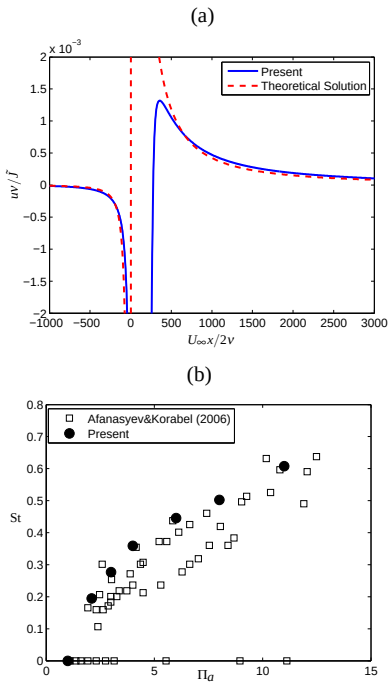

Figure 1. (a) Distribution of the streamwise velocity along the axis of 2D zero-momentum wake: Π_a = 1 and $\Pi_\nu = 50$. (b) Strouhal number versus Π_a.

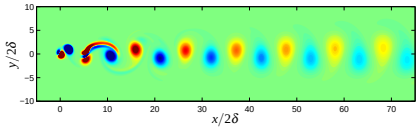

Figure 2. Contours of vorticity of 2D momentumless wake: Π_a = 11.0 and Π_ν = 230. Vorticity varies from $-0.2 \mid \omega_z \mid_{max}$ to $0.2 \mid \omega_z \mid_{max}$.

Table 1. Jet run parameters

Case	Domain size (in units of 2δ)	$N_x \times N_y \times N_z$
Unbounded domain	$-20 \leqslant x \leqslant 100$, $-16 \leqslant y \leqslant 16$, $-16 \leqslant z \leqslant 16$	$960 \times 256 \times 256$
Free surface	$-20 \leqslant x \leqslant 100$, $-32 \leqslant y \leqslant 32$, $-2 \leqslant z \leqslant 2$	$960 \times 512 \times 32$

Jet

We investigated the evolution and formation of a turbulent blob generated by an impulsive jet as a benchmark test case. The jet acts over a short time interval Δt_f with a forcing intensity J_T. The simulations are carried out for a jet Reynolds number of 2000 based on the forcing intensity; i.e. $Re_j = J_T^{1/2}/\nu$. The jet intensity is distributed to the computational grid via the 3D Gaussian function. To study the effect of a free surface, we consider two distinct canonical flows: a jet in an unbounded domain and a jet adjacent to a free surface. The number of grid cells and the domain size for both cases are documented in table 1. For the case of a jet interacting with a free surface, the forcing interval and the height of the computational domain were selected to correspond to the confinement number C of 2, at which the vortex dipole has been observed at the free surface (Voropayev *et al.*, 2007).

The transient evolution of the unbounded jet and the jet adjacent to a free surface is investigated using the second invariant of the velocity gradient tensor II (for details see Jeong & Hussain, 1995) and is shown in figure 3 and figure 4, respectively. The evolution of the momentum disturbance generated by an impulsive jet will be described below.

After the relatively strong jet $\left(Re_j \gg 1\right)$ is imparted into the fluid, it generates a turbulent jet with an azimuthal vorticity in the frontal region. The frontal region propagates away from its origin with propagation speed U_D, which is two times less than the local fluid velocity behind the front (Stern & Voropayev, 1984). Thus the turbulent jet enters into the vorticity front. At this stage, the ambient fluid entrains into the frontal region resulting in increasing the mass flux. Since the vertical growth of the turbulent blob is not restricted, the vertical and horizontal sizes of the blob increases while decreasing the propagation speed to conserve momentum. With time the turbulent blob transforms into a toroidal vortex (figure 3c).

When the vertical growth of the turbulent blob is suppressed by the stress-free layers, the frontal region can only expand horizontally due to the lateral entrainment (figure 4). A quasi-two-dimensional counter-rotating vortical structure is eventually formed at the late time.

The volume-integrated kinetic energy K of both cases is displayed in figure 5. The kinetic energy of the jet in an unbounded domain decreases faster than the jet suppressed by a free surface. This suggests that the toroidal vortex decays more rapidly than the vortex dipole.

Figure 9 illustrates the penetration of a momentum disturbance caused by an impulsive jet, visible at the free surface. Initially the concentrated momentum disturbance is ob-

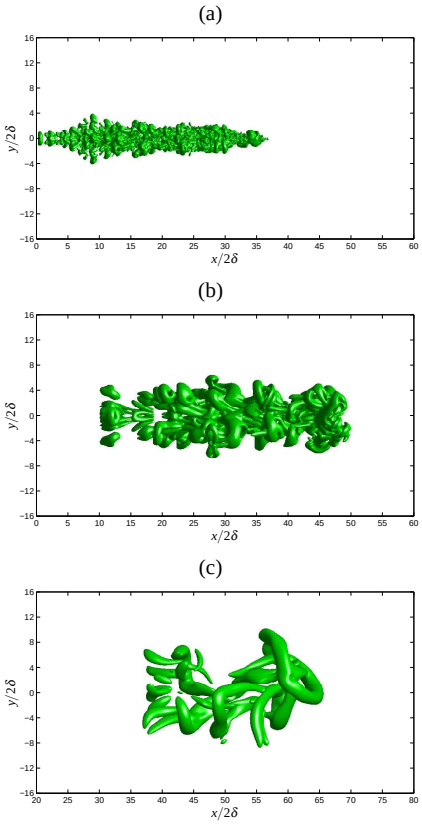

Figure 3. Top view of vortical structure of unbounded jet with level $\mathrm{II}\Delta t_f^2 = -0.008$: (a) $t/\Delta t_f = 2.5$, (b) $t/\Delta t_f = 12.5$, (c) $t/\Delta t_f = 62.5$.

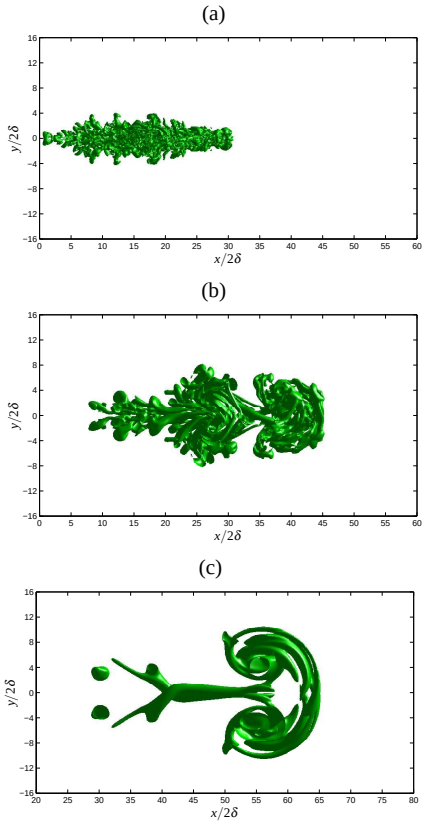

Figure 4. Top view of vortical structure of jet interacting with free surface with level $\mathrm{II}\Delta t_f^2 = -0.008$: (a) $t/\Delta t_f = 2.5$, (b) $t/\Delta t_f = 12.5$, (c) $t/\Delta t_f = 62.5$.

served without the formation of a vortex dipole (figure 9a). At this stage the intensity of the vertical vorticity at the free surface ω_z^* reaches its maximum (figure 6). With time the blob propagates away from its origin while increasing its horizontal size and decreasing its propagation speed, transforming into a quasi-planar dipole. During the process of dipole formation, the intensity of the vertical vorticity reduces as t^{-1}. The temporal evolution of the dipole propagation velocity U_D and the dipole radius R are showed in figures 7 and 8, respectively. It is found that the dipole speed decreases with time as $U_D \sim t^{-2/3}$, whilst its size increases as $R \sim t^{1/3}$. The power laws of the dipole in this simulation are same as those in the previous measurements in a linearly stratified fluid (Voropayev *et al.*, 1991) and in a shallow layer (Sous *et al.*, 2004; Voropayev *et al.*, 2007).

Manoeuvring-body wake

We selected a sphere with diameter D as a manoeuvring body. The Reynolds number based on the diameter and the terminal velocity of the sphere is $Re_D = UD/\nu = 1170$. The simulation was performed in the domain size of $-25D \leqslant x \leqslant 75D$, $-10D \leqslant y \leqslant 10D$ and $-1.25D \leqslant z \leqslant 1.25D$, with the number of grid cells $1280 \times 256 \times 32$.

At $t = 0$, the body accelerates from rest. At this stage, the thrust is greater than the drag leading to a momentum flux F transported to the fluid. After some time the body reaches its terminal speed and then moves with this constant speed.

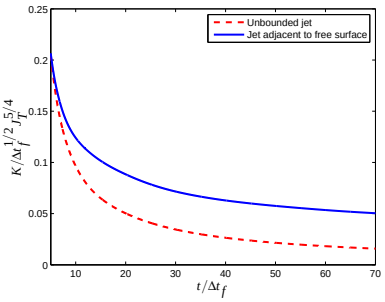

Figure 5. History of volume-integrated kinetic energy.

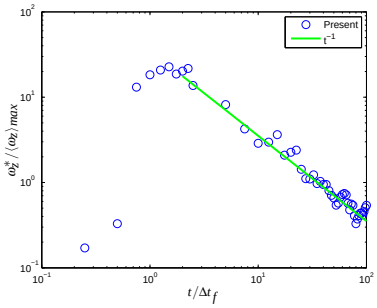

Figure 6. Decay of the maximum vertical vorticity at free surface.

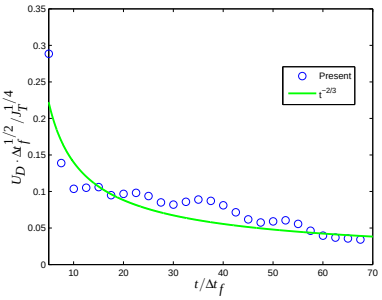

Figure 7. History of the dipole propagation velocity.

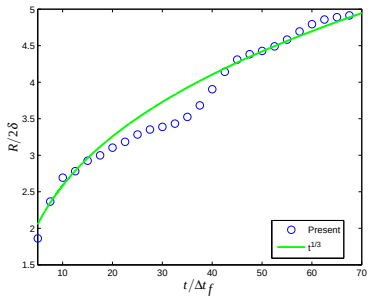

Figure 8. History of the dipole radius.

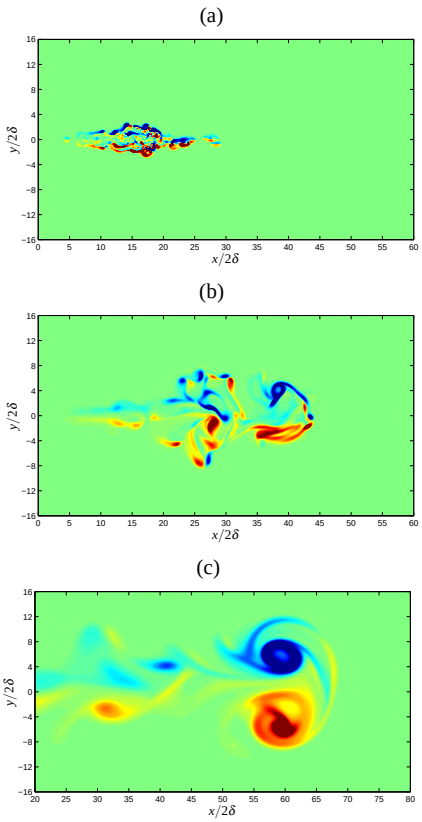

Figure 9. Contours of vorticity at free surface showing the penetration of the momentum source created by an impulsive jet: (a) $t/\Delta t_f = 2.5$, (b) $t/\Delta t_f = 12.5$, (c) $t/\Delta t_f = 75$. Vorticity varies from $-0.2 \mid \omega_z \mid_{max}$ to $0.2 \mid \omega_z \mid_{max}$.

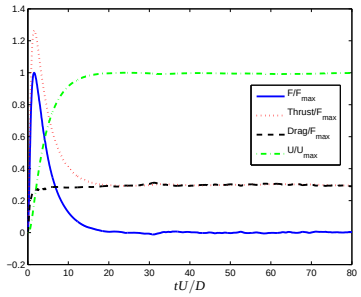

Figure 10. Histories of momentum flux, thrust, drag and speed of the body.

Histories of the momentum flux, the thrust, the drag and the velocity of the body are displayed in figure 10.

The second invariant of the velocity gradient tensor is used to visualise the vortical structure of the manoeuvring-body wake, as displayed in figure 11. It is found that a large-scale vortical structure, resulted from the acceleration of the body, appears in the late wake. The horizontal size of this vortical structure increases with time, due to lateral entrainment, whilst the vertical growth is restricted by the top and bottom free-slip walls. When the body is moving at constant speed, a momentumless wake is observed in the near field region. The zero-momentum wake decays very quickly without the formation of any coherent vortical structures.

Figure 12 shows the evolution of the vortical structure at the free surface. At early time, the momentum disturbance penetrates upward and produces its signature at the free surface. With time the horizontal eddy shows a gradual growth in size while it is propagating away from the body. It can be seen that the evolution of the momentum disturbance, created by an accelerating self-propelled body, at the beginning stage is similar to that generated by an impulsive jet (as shown in figure 9). Unfortunately, we could not observe a vortex dipole at the far wake presumably because the length of the computational domain in the streamwise direction is not long enough to capture the entire process of dipole formation. It can be seen from figure 4 that the jet-induced dipole is formed after about 60 jet duration times and the duration of acceleration for this case is around $15D/U$ (figure 10). Thus the time of eddy formation is of order $60 \times 15D/U = 900D/U$, corresponding to a domain length of approximately $1000D$ – i.e. roughly 13 times the current size.

SUMMARY

The formation and evolution of the momentum disturbance produced by both an impulsive jet and accelerating self-propelled body have been examined using DNS. It is found that when the momentum source is suppressed by the stress-free top and bottom layers, a quasi-planar counter-rotating structure is formed. The vortex dipole persists for a longer time compared to a typical toroidal vortex. Moreover, the characteristics of the dipole vortices induced by the presence of vertical confinement are similar to those in a stratified fluid. Future work will investigate how the impulsively submerged momentum disturbances are affected by and interact with a lower stratified layer.

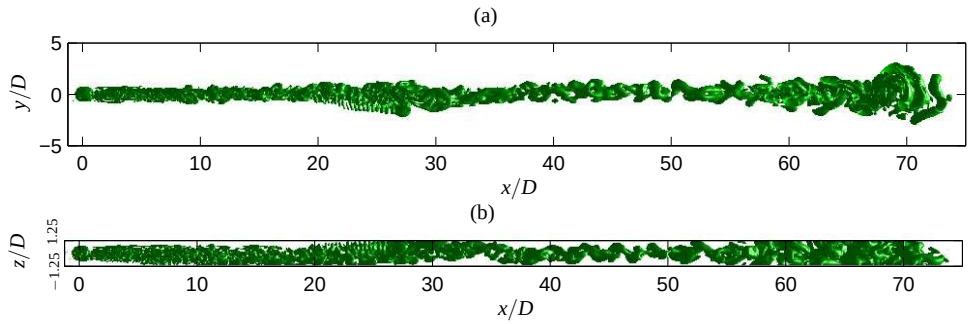

Figure 11. Vortical structure of manoeuvring-body wake at time $tU/D = 61.8$: (a) Top view, (b) Side view.

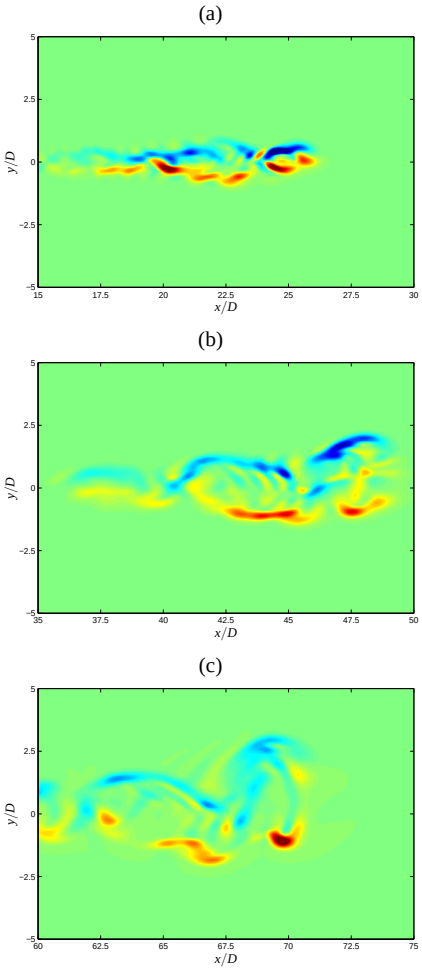

Figure 12. Contours of vorticity at free surface showing the penetration of wake signature of a manoeuvring self-propelled body: (a) $tU/D = 20.6$, (b) $tU/D = 41.2$, (c) $tU/D = 61.8$. Vorticity varies from -1.5 to 1.5.

ACKNOWLEDGMENTS

The authors gratefully acknowledge Prof Sergey Voropayev for his invaluable comments and suggestions. This work was funded by the UK Engineering and Physical Sciences Research Council (EPSRC) (Grant EP/G05035X), as part of the UK Turbulence Consortium (EP/G069581/1). The simulations were run on HECToR, the UK's national high-performance computing service.

REFERENCES

Afanasyev, Y. D. 2004 Wakes behind towed and self-propelled bodies: Asymptotic theory. *Phys. Fluids* **16** (8), 3235–3238.

Afanasyev, Y. D. & Korabel, V. N. 2006 Wakes and vortex streets generated by translating force and force doublet: Laboratory experiments. *J. Fluid Mech.* **553**, 119–141.

Ahlnäs, K., Royer, T. C. & George, T. H. 1987 Multiple dipole eddies in the alaska coastal current detected with landsat thematic mapper data. *J. Geophys. Res.* **92** (C12), 13041–13047.

Archer, P. J., Thomas, T. G. & Coleman, G. N. 2008 Direct numerical simulation of vortex ring evolution from the laminar to the early turbulent regime. *J. Fluid Mech.* **598**, 201–226.

Flór, J. B. & Van Heijst, G. J. F. 1994 An experimental study of dipolar vortex structures in a stratified fluid. *J. Fluid Mech.* **279**, 101–133.

Flór, J. B., Van Heijst, G. J. F. & Delfos, R. 1995 Decay of dipolar vortex structures in a stratified fluid. *Phys. Fluids* **7** (2), 374–383.

Jeong, J. & Hussain, F. 1995 On the identification of a vortex. *J. Fluid Mech.* **285**, 69–94.

Maxworthy, T. 1977 Some experimental studies of vortex rings. *J. Fluid Mech.* **81**, 465–495.

Roma, A M., Peskin, C S. & Berger, M J. 1999 An adaptive version of the immersed boundary method. *J. Comput. Phys.* **153** (2), 509–534.

Sous, D., Bonneton, N. & Sommeria, J. 2004 Turbulent vortex dipoles in a shallow water layer. *Phys. Fluids* **16** (8), 2886–2898.

Stern, M E. & Voropayev, S I. 1984 Formation of vorticity fronts in shear flow. *Phys. Fluids* **27** (4), 848–855.

Tennekes, H. & Lumley, J. L. 1972 *A First Course in Turbulence*. The MIT Press.

Voropayev, S. I., Afanasyev, Y D. & Filippov, I. A. 1991 Horizontal jets and vortex dipoles in a stratified fluid. *J. Fluid Mech.* **227**, 543–566.

Voropayev, S. I., Fernando, H. J. S., Smirnov, S. A. & Morrison, R. 2007 On surface signatures generated by submerged momentum sources. *Phys. Fluids* **19** (7), 076603.

Voropayev, S. I., McEachern, G. B., Fernando, H. J. S. & Boyer, D. L. 1999 Large vortex structures behind a maneuvering body in stratified fluids. *Phys. Fluids* **11** (6), 1682–1684.